

Article

Influence of Cr/Zr Ratio on Activity of Cr–Zr Oxide Catalysts in Non-Oxidative Propane Dehydrogenation

Alexander Zubkov, Tatiana Bugrova, Mikhail Salaev and Grigory Mamontov *

Laboratory of Catalytic Research, National Research Tomsk State University, 36 Lenin Ave., 634050 Tomsk, Russia; zubkov.chem@gmail.com (A.Z.); bugrova.tatiana@gmail.com (T.B.); mihan555@yandex.ru (M.S.)

* Correspondence: GrigoriyMamontov@mail.ru

Abstract: Two series of chromium–zirconium mixed oxide catalysts with different Cr/Zr molar ratio are prepared by co-precipitation method. Porous structure of the catalysts is studied by low-temperature N₂ adsorption–desorption. Phase composition and chromium states in the catalysts are characterized by X-ray diffraction (XRD), UV-visible spectroscopy, and temperature-programmed reduction with hydrogen (TPR-H₂). The mixed catalysts are tested in non-oxidative dehydrogenation of propane at 550 °C. The catalysts synthesized without ageing of precipitate show higher activity in propane dehydrogenation due to the higher content of reducible Cr^{+5/+6} species due to its stabilization on the ZrO₂ surface.

Keywords: chromia catalysts; mixed oxides; zirconia; dehydrogenation of propane



Citation: Zubkov, A.; Bugrova, T.; Salaev, M.; Mamontov, G. Influence of Cr/Zr Ratio on Activity of Cr–Zr Oxide Catalysts in Non-Oxidative Propane Dehydrogenation. *Crystals* **2021**, *11*, 1435. <https://doi.org/10.3390/crust11111435>

Academic Editors: Raghvendra Singh Yadav, Anju Anju and Shujun Zhang

Received: 30 October 2021
Accepted: 19 November 2021
Published: 22 November 2021

Publisher's Note: MDPI stays neutral with regard to jurisdictional claims in published maps and institutional affiliations.



Copyright: © 2021 by the authors. Licensee MDPI, Basel, Switzerland. This article is an open access article distributed under the terms and conditions of the Creative Commons Attribution (CC BY) license (<https://creativecommons.org/licenses/by/4.0/>).

1. Introduction

Catalytic technologies for dehydrogenation of hydrocarbons, especially propane and butanes, are among those environmentally benign approaches yielding important in-demand chemicals [1,2]. Among these chemicals is propylene, one of the most important raw materials for the petrochemical industry, used to manufacture polymers (e.g., polypropylene, polyacrylonitrile) and various commodity and value-added chemicals (e.g., acrolein, propylene oxide, acrylic acid) [3]. Presently, the catalytic dehydrogenation of paraffinic hydrocarbons is a promising way to produce olefins and is carried out through industrial approaches, including adiabatic fixed-bed (Catofin and Star), moving-bed (Olefex), and fluidized-bed (FBD) processes [4], with the Catofin and Oleflex technologies being most frequently used. Additionally, two main approaches are currently used for propane dehydrogenation, namely, direct non-oxidative (PDH) and oxidative (ODH) processes [5–8], with the latter group also utilizing a number of soft oxidants, e.g., CO₂, N₂O, halogens, and S-containing compounds [9–13].

The catalysts for dehydrogenation of paraffins mostly contain CrO_x [14–19] or Pt–Sn [20–23] as active components, while many other catalyst formulations, including but not limited to V [24,25], Ga [26], Co [27], Rh [28], Rh-Sn [29], zirconia-supported Rh, Ru, Pt or Ir [30], Pt-Ga [31], Pt-In [32], Pt-Ge [33], Pt-Pd [34], and TiO₂-supported catalysts with ZnO and ZrO₂ [35] have already shown their potential. Such composites are usually supported on various alumina or silica. While the latter feature more developed porous structure and show almost negligible activity in PDH reaction, they do not allow stabilizing Cr in highly oxidized states, resulting in the formation of α-Cr₂O₃ phase particles that are inactive in dehydrogenation [36]. Thus, the reduction of Cr content in the catalysts [37] and introduction of other supports that can act synergistically with the CrO_x species and other catalyst components [38] has been in focus, and the development of such catalysts has become a topical challenge.

Recently, ZrO₂ has become a promising candidate as a support for CrO_x-containing PDH catalysts [39–41]. This is connected with its capability to stabilize CrO_x species on the surface [42] and also with its own activity in dehydrogenation of hydrocarbons [43],

with monoclinic ZrO_2 showing a higher rate of propene formation and higher propene selectivity as compared to tetragonal zirconia. For bare zirconia, both catalyst activity and selectivity were higher as the crystallite sizes decreased, and for both monoclinic and tetragonal phases, the release of lattice oxygen during the reductive treatment resulted in the formation of coordinatively unsaturated Zr sites. Such Zr sites can also be formed under the influence of reaction conditions with the participation of active CrO_x species in Cr-Zr oxide catalysts [38] (or other dopants, e.g., Mg, Sm, and La [44]) and their silica-supported counterparts [42], resulting in efficient C–H bond activation [45]. The strength of interaction between CrO_x , ZrO_2 , and support as well as the sizes of zirconia crystallites in $CrZrO_x$ were found crucial for PDH performance. The crystallite sizes also controlled the concentration of oxygen vacancies. Weak CrO_x – SiO_2 interaction was found preferable, while the active species also increased the coke formation. For SiO_2 -supported $CrZrO_x$ -based composites, the zirconia crystallinity was shown to play an important role in propylene formation [46], with the increased crystallinity being beneficial for activity without selectivity loss.

The $CrZrO_x$ systems can be obtained by various methods, including impregnation of ZrO_2 with precursor of active ingredient (chromium (III) nitrate, ammonium dichromate) [47,48]. In this case, the catalyst surface is represented by highly dispersed species of the active component stabilized on the support, but the catalyst is characterized by a low specific surface area ($10\text{--}30\text{ m}^2/\text{g}$). Another promising approach is the preparation of mixed chromium and zirconium oxides using isolation from salt solutions, making it possible to obtain samples with a developed structure and high specific surface area [49]. Nevertheless, the peculiarities of the structure formation in Cr-Zr oxide catalysts depending on the changing of synthesis conditions, the effect of the Cr/Zr ratios on the phase composition, and the catalytic activity of such systems in the paraffin dehydrogenation have been poorly studied.

The present work is focused on the effect of synthesis conditions and the Cr/Zr molar ratio in mixed Cr-Zr oxides on the physical-chemical and catalytic properties of the resulting composites. The states of chromium on the surface and in the bulk of zirconium oxide are studied, and the catalysts are tested with nonoxidative propane dehydrogenation.

2. Materials and Methods

2.1. Catalysts Preparation

Two series of chromia–zirconia catalysts with different Cr/Zr molar ratio were prepared by co-precipitation method [26,50]. The required amounts of $ZrO(NO_3)_2 \cdot 2H_2O$ (chemically pure) and/or $Cr(NO_3)_3 \cdot 9H_2O$ (chemically pure) were dissolved in water. After that, an aqueous ammonia solution was added dropwise until $pH = 9$. The as-prepared or overnight-aged precipitates were filtered and washed by distilled water. Then, the prepared catalysts were dried at $100\text{ }^\circ\text{C}$ overnight and calcined at $600\text{ }^\circ\text{C}$ for 4 h. The reference sample Cr_2O_3 was synthesized by the thermal decomposition of $Cr(NO_3)_3 \cdot 9H_2O$ at $600\text{ }^\circ\text{C}$ for 4 h. The catalysts were denoted as $Cr_1Zr_{99}O_x$, $Cr_3Zr_{97}O_x$, $Cr_{10}Zr_{90}O_x$, and $Cr_{20}Zr_{80}O_x$, with the numbers standing for molar fraction of each metal and depending on the synthesis conditions with ageing, i.e., $CryZr_{1-y}O_x$ (aged), and without ageing, $(CryZr_{1-y}O_x)$.

2.2. Characterization

The porous structure was studied by the low-temperature adsorption–desorption of nitrogen at $-196\text{ }^\circ\text{C}$ using the TriStar 3020 analyzer (Micromeritics, Norcross, GA, USA). The specific surface area was determined using the multipoint Brunauer–Emmett–Teller (BET) method to rectify the adsorption isotherms in the P/P_0 range from 0.05 to 0.30. Pore size distributions were plotted using the Barrett–Joyner–Halenda method (BJH) with the analysis of adsorption branch of the isotherms. Prior to the measurements, the samples with mass of $\sim 200\text{ mg}$ were degassed under vacuum at $200\text{ }^\circ\text{C}$ for 2 h.

The phase composition was studied by X-ray diffraction (XRD) on the Rigaku Miniflex 600 (Rigaku Corporation, Tokyo, Japan) using a CuK_α -radiation source ($\lambda = 1.5418\text{ \AA}$) with monochromator. Conditions were as follows: rate was 2 degree/min, spacing was

0.2 degree/min, and angular range was $2\theta = 10\text{--}90^\circ$. The analysis of the phase composition was carried out using the database PCPDFWIN and full profile analysis program POWDER CELL 2.4. The size of the crystallites was calculated using the POWDER CELL 2.4 software according to the Scherrer equation:

$$D_{XRD} = K \cdot \lambda / \beta \cdot \cos\theta$$

where:

- D_{XRD} is the size of the ordered (crystalline) domains;
- K is a dimensionless shape factor, with a value close to unity;
- λ is the X-ray wavelength;
- β is the line broadening at half maximum intensity (FWHM).

Diffuse reflectance spectroscopy (DRS) analyses were performed on the Thermo Scientific Evolution 600 (Thermo Fisher Scientific, Waltham, MA, USA).

Reduction ability of the chromium oxides in the catalysts was studied by the temperature-programmed reduction in hydrogen (TPR-H₂). The TPR-H₂ was conducted using the AutoChem HP 2950 (Micromeritics, Norcross, GA, USA) with a thermal conductivity detector (TCD) ramping rate of 10 degree/min under a flow of argon–hydrogen (10% H₂/Ar) at a flow rate of 20 mL/min. To capture water produced during the reduction, a freezing trap was installed in front of the detector.

2.3. Catalytic Tests

Catalytic properties were studied in non-oxidative dehydrogenation of propane (PDH) to propylene. The samples were loaded into a flow-type tubular reactor with a quartz wool. The catalyst volume was 0.25 cm³, and the fraction was 0.25–0.5 mm. The catalysts were heated under a flow of N₂ (50 mL/min), then regenerated with air at 600 °C (50 mL/min) for 15 min and reduced under a flow of 15% H₂/N₂ for 5 min. After that, the dehydrogenation reaction occurred, and the sampling was carried out at 6 min. The catalyst was exposed to 15% C₃H₈/N₂ with a flow rate of 6 l/h (8000 h⁻¹) at 550 °C. The compositions of the obtained products were analyzed online by the Chromatek-Crystal gas chromatograph (CHROMATEC, Yoshkar-Ola, Mari El, Russia) with the Porapak Q capillary column, thermal conductivity detector (TCD), and flame ionization detector (FID). The components of the gas mixture were quantitatively determined using the Chromatek-Analyst software and the method of absolute calibration with a test gas mixture.

The activity of the catalysts was calculated as a space time yield (STY, kg/h·m³) taking into account the amount of converted propane (kg/h) per catalyst volume (m³). The turnover frequency (TOF) value was calculated as the rate of catalytic reaction per amount of chromium atoms.

$$TOF = V_{(C_3H_8)} \cdot C_{(C_3H_8)} \cdot P \cdot M_{(Cr)} / R \cdot T \cdot m_{(cat)} \cdot \varpi_{(Cr)}$$

where:

- $V_{(C_3H_8)}$ —volume rate of C₃H₈/N₂ gas mixture (m³/h);
- $C_{(C_3H_8)}$ —the C₃H₈ concentration in C₃H₈/N₂ gas mixture (0.15);
- P —pressure (Pa);
- $M_{(Cr)}$ —molar weight of chromium (52 g/mol);
- R —universal gas constant (8.314 m³ Pa/K · mol);
- T —reaction temperature (K);
- $m_{(cat)}$ —catalyst weight (g);
- $\varpi_{(Cr)}$ —Cr weight content in catalysts (g/g).

3. Results

According to the results of investigations by the method of low-temperature adsorption/desorption of nitrogen, all synthesized catalysts feature a mesoporous structure. Figure 1a,b shows the isotherms for catalysts synthesized by co-precipitation method with

and without ageing. For two series of catalysts, the presence of a hysteresis loop in the relative pressure range of 0.45–1.0 is characteristic and indicates the presence of small- and medium-sized mesopores. Figure 1a represents a pore size distribution (BJH). For the catalysts obtained without ageing, the pore size distribution is observed in the range from 2 to 21 nm, and with an increase in the chromium content, the distribution maximum is shifted from 2–30 nm to up to 2–9 nm.

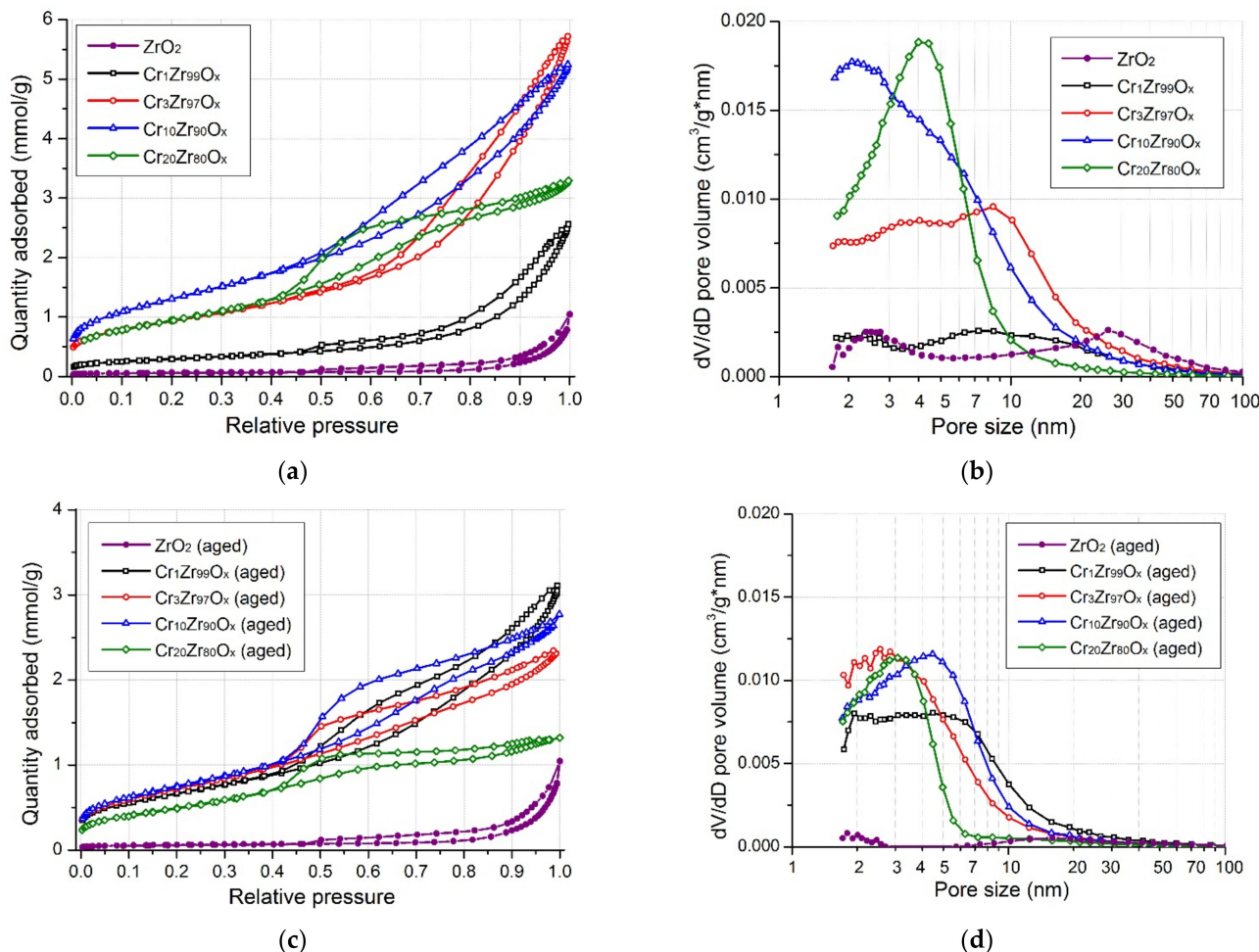


Figure 1. Nitrogen adsorption–desorption isotherms (a,c) and pore size distributions (b,d) for prepared catalysts: (a,b) without ageing, (c,d) with ageing of precipitate.

The differences in the pore size distribution for the mixed oxides within this series may be due to the different equilibrium sizes at time of deposition at different chromium content. Figure 1b shows the series with ageing characterized by a more uniform pore size distribution that is also shifted with an increasing chromium content, although in a more narrow range: from 2–8 nm to up to 2–4.5 nm.

Table 1 shows the textural characteristics for two series of mixed oxides prepared with and without ageing. The series without ageing is characterized by specific surface area growth with increasing chromium content. The specific surface area values for these systems vary from 24 m²/g (ZrO₂ (a)) to 107 m²/g (Cr₁₀Zr₉₀O_x (a)). Further increase in the Cr content to up to 20 mol.% leads to a decrease in the specific surface area (77 m²/g for Cr₂₀Zr₈₀O_x (a)). The values of the specific surface for the samples with ageing vary in the range 38 to 62 m²/g, and the one for ZrO₂ is 5 m²/g.

Table 1. Textural characteristics for two series of mixed oxides.

Sample	S_{BET} , m^2/g	V_p , cm^3/g	Sample	S_{BET} , m^2/g	V_p , cm^3/g	$\omega(\text{Cr})$, wt.%
ZrO_2	23	0.14	$\text{ZrO}_2(\text{aged})$	5	0.04	-
$\text{Cr}_1\text{Zr}_{99}\text{O}_x$	24	0.09	$\text{Cr}_1\text{Zr}_{99}\text{O}_x(\text{aged})$	54	0.11	0.4
$\text{Cr}_3\text{Zr}_{97}\text{O}_x$	76	0.20	$\text{Cr}_3\text{Zr}_{97}\text{O}_x(\text{aged})$	59	0.09	1.3
$\text{Cr}_{10}\text{Zr}_{90}\text{O}_x$	107	0.18	$\text{Cr}_{10}\text{Zr}_{90}\text{O}_x(\text{aged})$	62	0.10	4.4
$\text{Cr}_{20}\text{Zr}_{80}\text{O}_x$	77	0.11	$\text{Cr}_{20}\text{Zr}_{80}\text{O}_x(\text{aged})$	42	0.05	9.2

Figure 2 shows the XRD patterns for the obtained samples. According to the XRD results (Figure 2 and Table 2), a mixture of monoclinic and tetragonal phase of ZrO_2 is observed for the ZrO_2 supports. The increase in the chromium content in the catalyst leads to ZrO_2 stabilization, mainly in the tetragonal modification. The tetragonal ZrO_2 phase in the mixed oxides obtained with ageing prevails even at low chromium contents, while the $\text{Cr}_1\text{Zr}_{99}\text{O}_x$ - $\text{Cr}_3\text{Zr}_{90}\text{O}_x$ samples without ageing mainly contain the monoclinic ZrO_2 phase.

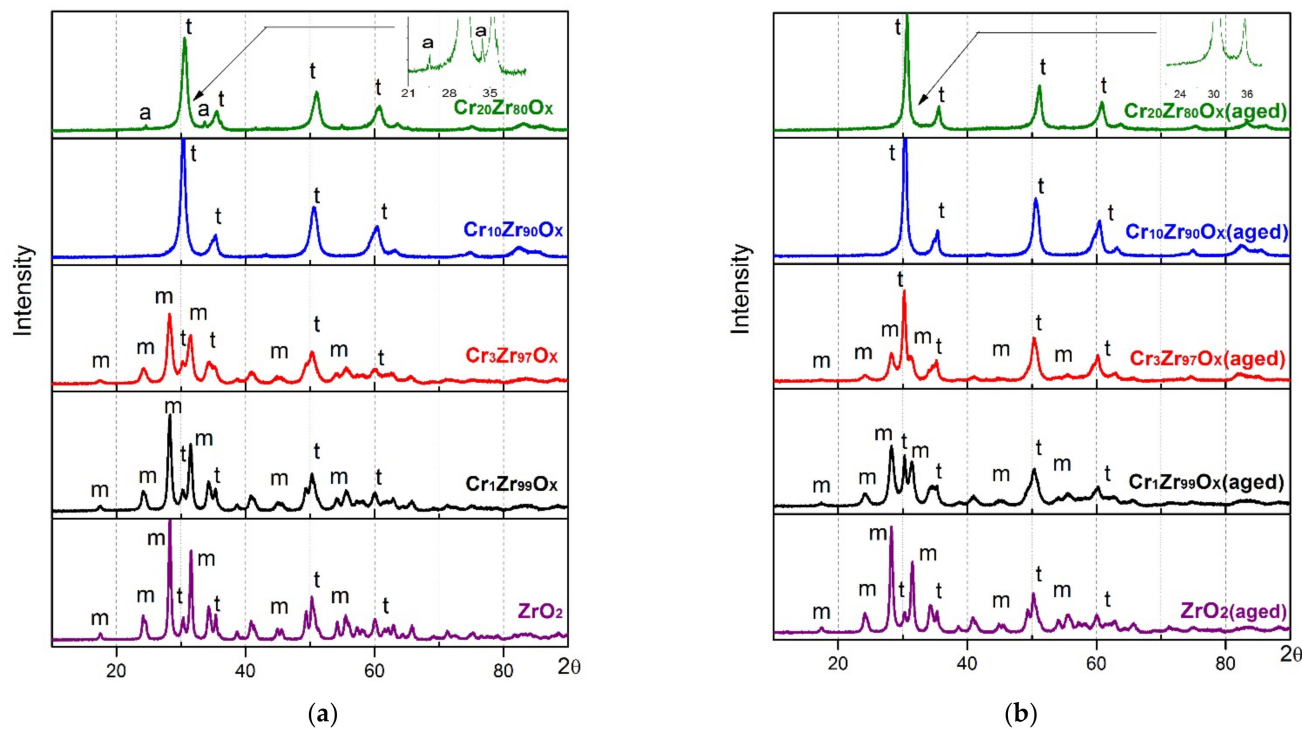


Figure 2. XRD patterns for Cr-Zr mixed oxide samples prepared (a) without and (b) with ageing of precipitate: m—monoclinic ZrO_2 phase, t—tetragonal ZrO_2 phase, a— $\alpha\text{-Cr}_2\text{O}_3$.

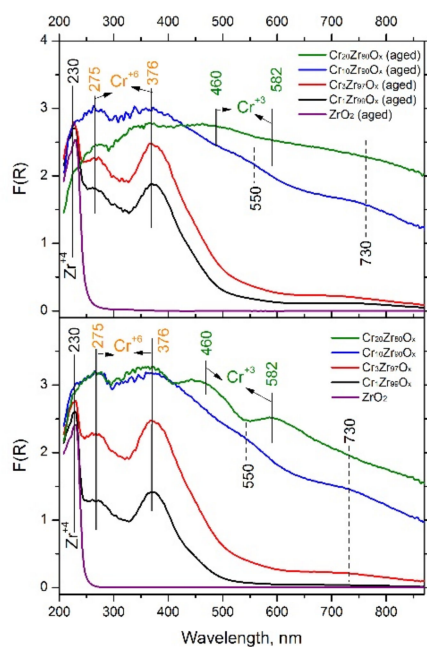
The absence of reflections of the Cr-containing phases indicates the stabilization of chromia in a highly dispersed state. The reflections of $\alpha\text{-Cr}_2\text{O}_3$ were found only in the $\text{Cr}_{20}\text{Zr}_{80}\text{O}_x$ catalyst (without ageing). This is attributed to the high Cr loading. The aging of the $\text{Cr}_{20}\text{Zr}_{80}\text{O}_x$ catalyst leads to the disappearance of reflections of $\alpha\text{-Cr}_2\text{O}_3$ phase (insertion in Figure 2b), which indicates chromia redistribution during the precipitate adding. The precipitate ageing leads to both increase in the size of ZrO_2 crystallites and changing of the cell parameter of ZrO_2 phases (Table 2). The shift in the t- ZrO_2 phase reflections towards large angles with high chromium contents in the catalysts may be due to the incorporation of chromium ions into zirconia lattice, with the corresponding decreasing of the cell parameter from 3.603–3.600 Å to 3.567–3.570 Å for $\text{Cr}_{20}\text{Zr}_{80}\text{O}_x$ sample (parameter a in Table 2).

Table 2. The XRD results.

Sample	Phases	ω , wt. %	D_{XRD} , nm	a , Å	Sample	Phases	ω , wt. %	D_{XRD} , nm	a , Å
ZrO ₂	m-ZrO ₂	92.32	20.2	-	(aged)	ZrO ₂	90.67	17.3	5.147
	t-ZrO ₂	7.68	18.1	-		t-ZrO ₂	9.33	15.4	3.600
Cr ₁ Zr ₉₉ O _x	m-ZrO ₂	91.50	13.5	5.147	Cr ₁ Zr ₉₉ O _x (aged)	m-ZrO ₂	79.45	8.95	5.157
	t-ZrO ₂	8.50	12.8	3.603		t-ZrO ₂	20.55	19.9	3.597
Cr ₃ Zr ₉₇ O _x	m-ZrO ₂	90.26	9.3	5.151	Cr ₃ Zr ₉₇ O _x (aged)	m-ZrO ₂	48.75	3.33	5.152
	t-ZrO ₂	9.74	7.9	3.603		t-ZrO ₂	51.25	17.3	3.599
Cr ₁₀ Zr ₉₀ O _x	m-ZrO ₂	0	-	-	Cr ₁₀ Zr ₉₀ O _x (aged)	m-ZrO ₂	0	-	-
	t-ZrO ₂	100	11.4	3.588		t-ZrO ₂	100	17.1	3.587
Cr ₂₀ Zr ₈₀ O _x	a-Cr ₂ O ₃	7.22	-	-	Cr ₂₀ Zr ₈₀ O _x (aged)	m-ZrO ₂	0	-	-
	t-ZrO ₂	92.78	9.6	3.570		t-ZrO ₂	100	14.7	3.567

Thus, according to the XRD results, the Cr/Zr ratio in the mixed Cr–Zr oxide catalysts significantly affects the phase composition. Increasing the Cr content leads to stabilization of tetragonal ZrO₂ phase, which is attributed to the Cr incorporation into this phase. The size of the t-ZrO₂ crystallites is smaller with the increasing Cr loading. The aging of the precipitate influences both the phase composition of catalysts and the size of crystallites. The precipitate aging leads to the increasing of the crystallites' size and the increased amount of tetragonal ZrO₂ phase that is associated with the chromia redistribution and t-ZrO₂ stabilization due to the incorporation of Cr atoms into zirconia lattice. The changing of the phase composition and increased size of the crystallites lead to the decreasing of S_{BET} and pore volume (Table 1).

The chemical state of chromium on the surface of ZrO₂ was studied by the DRS method, and Figure 3 shows the diffuse reflectance spectra for the mixed oxides. The onset of the linear increase in the diffuse reflectance spectrum is taken as a measure of the forbidden gap that occurs at around 230 nm. This is a characteristic of the end of the bulk tetragonal zirconia phase. All samples are characterized by the intensive absorption bands at 280 and 370 nm, attributed to the ligand-to-metal charge transfer for the Cr⁺⁶ cations in the tetrahedral oxygen symmetry.

**Figure 3.** DRS spectra for CrZrO_x catalysts synthesized with and without ageing of precipitate.

The absorption bands with maxima at 470 and 580 nm in the spectrum for the $\text{Cr}_{20}\text{Zr}_{80}\text{O}_x$ (a) catalyst can be attributed to $\text{A}_{2g} \rightarrow \text{T}_{1g}$ and $\text{A}_{2g} \rightarrow \text{T}_{2g}$ Cr(III) transitions in octahedral symmetry [20,29], which is consistent with the XRD results. For the samples with Cr content from 1.3 to 4.4/9.2 wt.%, the DRS spectra contain non-intensive absorption bands at 550 and 730 nm. According to the literature, these absorption bands may be due to the appearance of the resonant d-d transition of the Cr^{3+} cations [51] or due to the presence of the small content of Cr^{5+} ions in the octahedral oxygen coordination [52].

The TPR-H₂ profiles (Figure 4) for all catalysts contain two broad peaks of hydrogen consumption, with the temperature maxima at 351–383 and 488–535 °C. These peaks can be attributed to the $\text{Cr}^{5+/6}$ reduction into Cr^{3+} , since the intensity of these peaks increases as the Cr content rises [30].

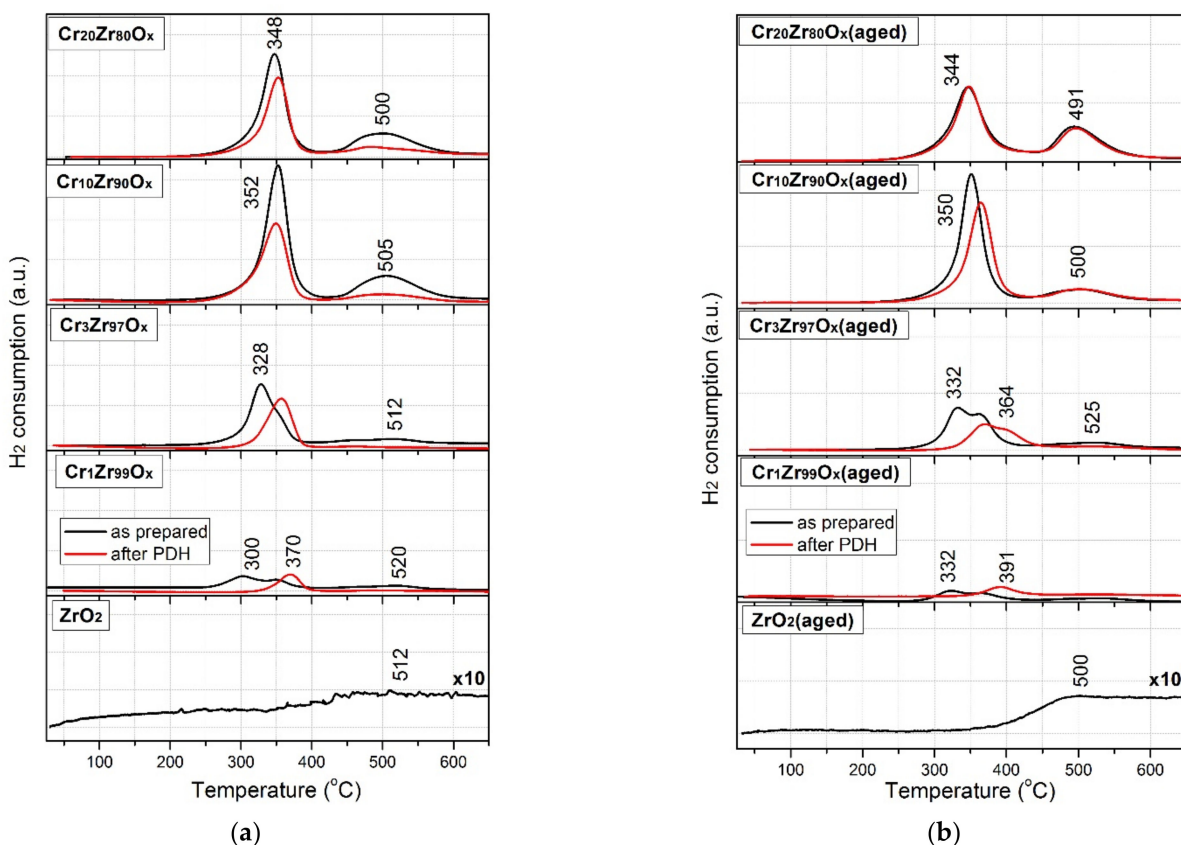


Figure 4. TPR-H₂ profiles for ZrO_2 and CrZrO_x catalysts: catalysts (a) without ageing, (b) with ageing of precipitate.

However, the second consumption peak can also be attributed to the ZrO_2 reduction, and an increase in its intensity corresponds to an increase in the number of defects in ZrO_2 structure with enrichment in the chromium content. The TPR-H₂ for ZrO_2 samples are characterized by the presence of the H₂ consumption peak at ~500 °C, but its intensity is relatively low. It is noteworthy that for the series obtained without aging, the intensity of this high-temperature peak after the catalytic experiment is significantly reduced.

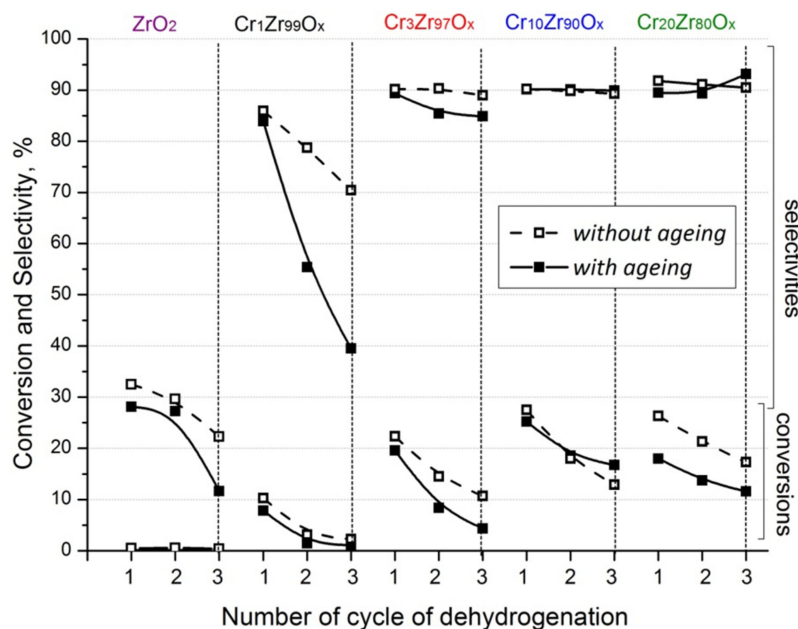
Table 3 represents the quantification of the hydrogen consumed in the TPR experiments as well as the amount of maximal theoretical H₂ consumption corresponding to the reduction of all Cr^{6+} chromium into Cr^{3+} . The values of H₂ consumption for $\text{Cr}_1\text{Zr}_{99}\text{O}_x$ and $\text{Cr}_3\text{Zr}_{97}\text{O}_x$ catalysts are close to the theoretical consumption, which indicates the chromium stabilization on the surface of catalysts predominantly as Cr^{6+} species. The highest reduction ability (722 $\mu\text{mol/g}$) is observed for $\text{Cr}_{10}\text{Zr}_{90}\text{O}_x$ catalyst. The decreased hydrogen consumption for $\text{Cr}_{20}\text{Zr}_{80}\text{O}_x$ samples can be attributed to both the formation of α- Cr_2O_3 phase and a significant incorporation of Cr^{3+} species into the zirconia lattice.

Table 3. H₂ consumption for obtained catalysts.

Sample	before PDH		Sample	before PDH		H ₂ , μmol/g (Cr ⁶⁺ → Cr ³⁺)
	n(H ₂), μmol/g	after PDH		n(H ₂), μmol/g	after PDH	
ZrO ₂	-	-	ZrO ₂ (aged)	-	-	-
Cr ₁ Zr ₉₉ O _x	132	98	Cr ₁ Zr ₉₉ O _x (aged)	108	72	122
Cr ₃ Zr ₉₇ O _x	345	218	Cr ₃ Zr ₉₇ O _x (aged)	318	207	369
Cr ₁₀ Zr ₉₀ O _x	722	442	Cr ₁₀ Zr ₉₀ O _x (aged)	581	514	1266
Cr ₂₀ Zr ₈₀ O _x	670	466	Cr ₂₀ Zr ₈₀ O _x (aged)	601	537	2637

Table 3 also shows that the amount of consumed H₂ for the catalysts after propane dehydrogenation (PDH) is lower than for the as-prepared catalysts. This indicates the decreased amount of reversibly oxidized/reduced Cr^{6+/3+} species in the catalytic process that may also be attributed to the Cr³⁺ incorporation into the zirconia lattice.

The catalytic properties of the synthesized catalysts were tested with the reaction of non-oxidative propane dehydrogenation. Figure 5 shows the obtained conversion and selectivity values in three cycles of PDH with sampling at 6 min. The activity of the catalysts obtained without ageing gradually increases as the chromium content rises: Cr₁Zr₉₉O_x < Cr₃Zr₉₇O_x < Cr₁₀Zr₉₀O_x. Table 4 summarizes the space time yield (STY) and turnover frequencies (TOF). The conversion and selectivity values for the Cr₂₀Zr₈₀O_x catalyst are similar to those for Cr₁₀Zr₉₀O_x. However, the stability of the sample during three cycles is higher.

**Figure 5.** Catalytic results for obtained samples in PDH.

For the catalysts obtained with ageing, the conversion and productivity are observed to increase with an increase in the active component content. The sample Cr₁₀Zr₉₀O_x shows the highest conversion and selectivity. The activity decreased with an increase in the Cr content in the series with ageing to up to Cr₂₀Zr₈₀O_x (aged). The Cr₁₀Zr₉₀O_x samples obtained without and with ageing feature the highest rate of propene formation in the reaction of propane dehydrogenation, which is consistent with the TPR results.

Table 4. STY and TOF for obtained sample during three cycles.

Sample	STY, kg/h·m ³			TOF, h ⁻¹		
	Cycle 1	Cycle 2	Cycle 3	Cycle 1	Cycle 2	Cycle 3
ZrO ₂	8	8	5	-	-	-
Cr ₁ Zr ₉₉ O _x	857	238	155	259	78	57
Cr ₃ Zr ₉₇ O _x	1955	1274	922	196	127	94
Cr ₁₀ Zr ₉₀ O _x	2409	1572	1117	78	51	36
Cr ₂₀ Zr ₈₀ O _y	2344	1889	1520	33	27	22
ZrO ₂ (aged)	15	16	9	-	-	-
Cr ₁ Zr ₉₉ O _x (aged)	639	78	42	198	37	28
Cr ₃ Zr ₉₇ O _x (aged)	1700	694	360	172	74	38
Cr ₁₀ Zr ₉₀ O _x (aged)	2209	1628	1464	41	30	27
Cr ₂₀ Zr ₈₀ O _y (aged)	1565	1193	1050	10	8	7

4. Discussion

Two series of aged and non-aged Cr-Zr oxidative catalysts were prepared, and the catalyst series differed from each other in their structural and phase characteristics. The low-temperature nitrogen adsorption method determines more advanced porous structure of the non-aged catalysts. The obtained XRD results describe the phase composition function of the Cr/Zr ratio. Increasing of the chromium content leads to stabilization of the tetragonal zirconium oxide (IV). The α -Cr₂O₃ phase is detected only for Cr₂₀Zr₈₀O_y catalyst with high Cr content. According to the UV-vis spectroscopy data, Cr is stabilized as Cr(VI) in the highly dispersed state. The TPR results confirm the presence of Cr(VI) and its reduction in the reductive atmosphere into Cr(III). The amount of redox Cr(VI/III) species is higher for the catalysts prepared without precipitate ageing.

Furthermore, the above-mentioned catalyst series is more reactive in propane dehydrogenation, which can be explained by higher surface area and higher amount of highly dispersed redox CrO_x species. The highest activity is observed for Cr₁₀Zr₉₀O_x catalysts that also feature the highest amount of H₂ consumed in TPR. Thus, the activity correlates with the amount of redox Cr⁶⁺ species in the catalyst. The TOF value is highest for Cr₁Zr₉₉O_x and Cr₃Zr₉₇O_x catalysts, which may be attributed to high dispersion of these Cr⁶⁺ (and probably Cr⁵⁺) species and minimal amount of Cr species incorporated into the zirconia structure. Probably, the activity of the catalysts is attributable to both chromia and zirconia active species in the CrZrO_x catalysts, but the pristine ZrO₂ sample is characterized by rather low activity.

5. Conclusions

Thus, the influence of the Cr/Zr ratio and he precipitate ageing was shown for the CrZrO_x catalysts for non-oxidative propane dehydrogenation. The precipitate ageing had a negative influence on the activity of CrZrO_x catalysts with low Cr loading. In the case of Cr₁₀Zr₉₀O_y and Cr₂₀Zr₈₀O_y catalysts, the stability of the catalysts with precipitate ageing was higher. The highest activity was found for the Cr₁₀Zr₉₀O_y catalyst.

Author Contributions: Conceptualization, G.M. and T.B.; investigation, A.Z. and T.B.; resources, G.M.; writing—original draft preparation, A.Z. and T.B.; writing—review and editing, M.S. and G.M.; visualization, T.B. and M.S.; supervision, G.M.; project administration, G.M.; funding acquisition, G.M. All authors have read and agreed to the published version of the manuscript.

Funding: This work was carried out within the framework of the state assignment of the Ministry of Science and Higher Education of the Russian Federation (project No. 0721-2020-0037).

Institutional Review Board Statement: Not applicable.

Informed Consent Statement: Not applicable.

Conflicts of Interest: The authors declare no conflict of interest.

References

1. Otroshchenko, T.; Jiang, G.; Kondratenko, V.A.; Rodemerck, U.; Kondratenko, E.V. Current status and perspectives in oxidative, non-oxidative and CO₂-mediated dehydrogenation of propane and isobutane over metal oxide catalysts. *Chem. Soc. Rev.* **2021**, *50*, 473–527. [[CrossRef](#)]
2. Sattler, J.J.; Ruiz-Martinez, J.; Santillan-Jimenez, E.; Weckhuysen, B.M. Catalytic dehydrogenation of light alkanes on metals and metal oxides. *Chem. Rev.* **2014**, *114*, 10613–10653. [[CrossRef](#)]
3. Dai, Y.; Gao, X.; Wang, Q.; Wan, X.; Zhou, C.; Yang, Y. Recent progress in heterogeneous metal and metal oxide catalysts for direct dehydrogenation of ethane and propane. *Chem. Soc. Rev.* **2021**, *50*, 5590–5630. [[CrossRef](#)]
4. Monai, M.; Gambino, M.; Wannakao, S.; Weckhuysen, B.M. Propane to olefins tandem catalysis: A selective route towards light olefins production. *Chem. Soc. Rev.* **2021**, *50*, 11503–11529. [[CrossRef](#)] [[PubMed](#)]
5. Lawson, S.; Farsad, A.; Adebayo, B.; Newport, K.; Schueddig, K.; Lowrey, E.; Polo-Garzon, F.; Rezaei, F.; Rownaghi, A.A. A Novel Method of 3D Printing High-Loaded Oxide/H-ZSM-5 Catalyst Monoliths for Carbon Dioxide Reduction in Tandem with Propane Dehydrogenation. *Adv. Sustain. Syst.* **2021**, *5*, 2000257. [[CrossRef](#)]
6. De Oliveira, J.F.S.; Volanti, D.P.; Bueno, J.M.C.; Ferreira, A.P. Effect of CO₂ in the oxidative dehydrogenation reaction of propane over Cr/ZrO₂ catalysts. *Appl. Catal. A Gen.* **2018**, *558*, 55–66. [[CrossRef](#)]
7. Kharlamova, T.S.; Timofeev, K.L.; Salaev, M.A.; Svetlichnyi, V.A.; Vodyankina, O.V. Monolayer MgVO_x/Al₂O₃ catalysts for propane oxidative dehydrogenation: Insights into a role of structural, redox, and acid-base properties in catalytic performance. *Appl. Catal. A Gen.* **2020**, *59825*, 117574. [[CrossRef](#)]
8. Kharlamova, T.; Sushchenko, E.; Izaak, T.; Vodyankina, O. Phase composition, structural peculiarities and catalytic properties of supported MgO-V₂O₅/Al₂O₃ catalysts for oxidative dehydrogenation of propane: Insight into formation of surface Mg-V-O phase. *Catal. Today* **2016**, *278*, 174–184. [[CrossRef](#)]
9. Jiang, X.; Sharma, L.; Fung, V.; Park, S.J.; Jones, C.W.; Sumpter, B.G.; Baltrusaitis, J.; Wu, Z. Oxidative dehydrogenation of propane to propylene with soft oxidants via heterogeneous catalysis. *ACS Catal.* **2021**, *11*, 2182–2234. [[CrossRef](#)]
10. Wu, R.; Xie, P.; Cheng, Y.; Yue, Y.; Gu, S.; Yang, W.; Miao, C.; Hua, W.; Gao, Z. Hydrothermally prepared Cr₂O₃–ZrO₂ as a novel efficient catalyst for dehydrogenation of propane with CO₂. *Catal. Commun.* **2013**, *39*, 20–23. [[CrossRef](#)]
11. Bugrova, T.A.; Dutov, V.V.; Svetlichnyi, V.A.; Cortés Corberán, V.; Mamontov, G.V. Oxidative dehydrogenation of ethane with CO₂ over CrO_x catalysts supported on Al₂O₃, ZrO₂, CeO₂ and Ce_xZr_{1-x}O₂. *Catal. Today* **2019**, *333*, 71–80. [[CrossRef](#)]
12. Rahmani, F.; Haghghi, M.; Mohammadkhani, B. Enhanced dispersion of Cr nanoparticles over nanostructured ZrO₂-doped ZSM-5 used in CO₂-oxydehydrogenation of ethane. *Microp. Mesopor. Mater.* **2017**, *242*, 34–49. [[CrossRef](#)]
13. Gao, Y.; Jie, X.; Wang, C.; Jacobs, R.M.J.; Li, W.; Yao, B.; Dilworth, J.R.; Xiao, T.; Edwards, P.P. One-Pot Synthesis of Ca Oxide-Promoted Cr Catalysts for the Dehydrogenation of Propane Using CO₂. *Ind. Eng. Chem. Res.* **2020**, *59*, 12645–12656. [[CrossRef](#)]
14. Hu, Z.-P.; Wang, Z.; Yuan, Z.-Y. Cr/Al₂O₃ catalysts with strong metal-support interactions for stable catalytic dehydrogenation of propane to propylene. *Molec. Catal.* **2020**, *493*, 111052. [[CrossRef](#)]
15. Nazimov, D.A.; Klimov, O.V.; Saiko, A.V.; Trukhan, S.N.; Glazneva, T.S.; Prosvirin, I.P.; Cherepanova, S.V.; Noskov, A.S. Effect of the K loading on effective activation energy of isobutane dehydrogenation over chromia/alumina catalysts. *Catal. Today* **2021**, *375*, 401–409. [[CrossRef](#)]
16. Nazimov, D.A.; Klimov, O.V.; Danilova, I.G.; Trukhan, S.N.; Saiko, A.V.; Cherepanova, S.V.; Chesalov, Y.A.; Martyanov, O.N.; Noskov, A.S. Effect of alumina polymorph on the dehydrogenation activity of supported chromia/alumina catalysts. *J. Catal.* **2020**, *391*, 35–47. [[CrossRef](#)]
17. Zolotukhina, A.I.; Romanova, E.V.; Bugrova, T.A.; Knyazev, A.S.; Mamontov, G.V. Influence of impregnation conditions on the activity of CrO_x/Al₂O₃ catalysts in dehydrogenation of isobutane in fixed bed reactor. *Arab. J. Chem.* **2020**, *13*, 9130–9138. [[CrossRef](#)]
18. Salaeva, A.A.; Salaev, M.A.; Vodyankina, O.V.; Mamontov, G.V. Synergistic effect of Cu and Zn modifiers on the activity of CrO_x/Al₂O₃ catalysts in isobutane dehydrogenation. *Appl. Catal. A Gen.* **2019**, *581*, 82–90. [[CrossRef](#)]
19. Salaeva, A.A.; Salaev, M.A.; Mamontov, G.V. Effect of Cu modifier on the performance of CrO_x/Al₂O₃ catalysts for isobutane dehydrogenation. *Chem. Eng. Sci.* **2020**, *2156*, 115462. [[CrossRef](#)]
20. Xu, Z.; Xu, R.; Yue, Y.; Yuan, P.; Bao, X.; Abou-Hamad, E.; Basset, J.-M.; Zhu, H. Bimetallic Pt–Sn nanocluster from the hydrogenolysis of a well-defined surface compound consisting of [(=AlO–)Pt(COD)Me] and [(=AlO–)SnPh₃] fragments for propane dehydrogenation. *J. Catal.* **2019**, *374*, 391–400. [[CrossRef](#)]
21. Natarajan, P.; Khan, H.A.; Yoon, S.; Jung, K.-D. One-pot synthesis of Pt–Sn bimetallic mesoporous alumina catalysts with worm-like pore structure for n-butane dehydrogenation. *J. Ind. Eng. Chem.* **2018**, *63*, 380–390. [[CrossRef](#)]
22. Pham, H.N.; Sattler, J.J.H.B.; Weckhuysen, B.M.; Datye, A.K. Role of Sn in the regeneration of Pt/γ-Al₂O₃ light alkane dehydrogenation catalysts. *ACS Catal.* **2016**, *6*, 2257–2264. [[CrossRef](#)]
23. Srinath, N.V.; Poelman, H.; Buelens, L.; Dendooven, J.; Reyniers, M.-F.; Marin, G.B.; Galvita, V.V. Behaviour of Platinum-Tin during CO₂-assisted propane dehydrogenation: Insights from quick X-ray absorption spectroscopy. *J. Catal.* **2021**. [[CrossRef](#)]

24. Rodemerck, U.; Stoyanova, M.; Kondratenko, E.V.; Linke, D. Influence of the kind of VO_x structures in $\text{VO}_x/\text{MCM}-41$ on activity, selectivity and stability in dehydrogenation of propane and isobutane. *J. Catal.* **2017**, *352*, 256–263. [[CrossRef](#)]
25. Jeon, N.; Choe, H.; Jeong, B.; Yun, Y. Propane dehydrogenation over vanadium-doped zirconium oxide catalysts. *Catal. Today* **2020**, *352*, 337–344. [[CrossRef](#)]
26. Matveyeva, A.N.; Wärnå, J.; Pakhomov, N.A.; Murzin, D.Y. Kinetic modeling of isobutane dehydrogenation over $\text{Ga}_2\text{O}_3/\text{Al}_2\text{O}_3$ catalyst. *Chem. Eng. J.* **2020**, *381*, 122741. [[CrossRef](#)]
27. Dai, Y.; Gu, J.; Tian, S.; Wu, Y.; Chen, J.; Li, F.; Du, Y.; Peng, L.; Ding, W.; Yang, Y. $\gamma\text{-Al}_2\text{O}_3$ sheet-stabilized isolate Co^{2+} for catalytic propane dehydrogenation. *J. Catal.* **2020**, *381*, 482–492. [[CrossRef](#)]
28. Zhang, Y.; Zhao, Y.; Otroshchenko, T.; Perechodjuk, A.; Kondratenko, V.A.; Bartling, S.; Rodemerck, U.; Linke, D.; Jiao, H.; Jiang, G.; et al. Structure-Activity-Selectivity Relationships in Propane Dehydrogenation over Rh/ZrO_2 catalysts. *ACS Catal.* **2020**, *10*, 6377–6388. [[CrossRef](#)]
29. Natarajan, P.; Khan, H.A.; Jaleel, A.; Park, D.S.; Kang, D.-C.; Yoon, S.; Jung, K.-D. The pronounced effect of Sn on RhSn catalysts for propane dehydrogenation. *J. Catal.* **2020**, *392*, 8–20. [[CrossRef](#)]
30. Perechodjuk, A.; Zhang, Y.; Kondratenko, V.A.; Rodemerck, U.; Linke, D.; Bartling, S.; Kreyenschulte, C.R.; Jiang, G.; Kondratenko, E.V. The effect of supported Rh, Ru, Pt or Ir nanoparticles on activity and selectivity of ZrO_2 -based catalysts in non-oxidative dehydrogenation of propane. *Appl. Catal. A Gen.* **2020**, *60225*, 117731. [[CrossRef](#)]
31. Wang, P.; Yao, J.; Jiang, Q.; Gao, X.; Lin, D.; Yang, H.; Wu, L.; Tang, Y.; Tan, L. Stabilizing the Isolated Pt Sites on $\text{PtGa}/\text{Al}_2\text{O}_3$ Catalyst via Silica Coating Layers for Propane Dehydrogenation at Low Temperature. *Appl. Catal. B Environ.* **2022**, *300*, 120731. [[CrossRef](#)]
32. Tolek, W.; Suriye, K.; Prasertthdam, P.; Panpranot, J. Effect of preparation method on the Pt-In modified $\text{Mg}(\text{Al})\text{O}$ catalysts over dehydrogenation of propane. *Catal. Today* **2020**, *358*, 100–108. [[CrossRef](#)]
33. Rimaz, S.; Chen, L.; Monzón, A.; Kawi, S.; Borgna, A. Enhanced selectivity and stability of $\text{Pt-Ge}/\text{Al}_2\text{O}_3$ catalysts by Ca promotion in propane dehydrogenation. *Chem. Eng. J.* **2021**, *405*, 126656. [[CrossRef](#)]
34. Saxena, R.; De, M. Enhanced performance of supported Pd-Pt bimetallic catalysts prepared by modified electroless deposition for butane dehydrogenation. *Appl. Catal. A Gen.* **2021**, *610*, 117933. [[CrossRef](#)]
35. Han, S.; Zhao, D.; Lund, H.; Rockstroh, N.; Bartling, S.; Doronkin, D.E.; Grunwaldt, J.-D.; Gao, M.; Jiang, G.; Kondratenko, E.V. TiO_2 -Supported catalysts with ZnO and ZrO_2 for non-oxidative dehydrogenation of propane: Mechanistic analysis and application potential. *Catal. Sci. Technol.* **2020**, *10*, 7046–7055. [[CrossRef](#)]
36. Takehira, K.; Ohishi, Y.; Shishido, T.; Kawabata, T.; Takaki, K.; Zhang, Q.; Wang, Y. Behavior of active sites on Cr-MCM-41 catalysts during the dehydrogenation of propane with CO_2 . *J. Catal.* **2004**, *224*, 404–416. [[CrossRef](#)]
37. Otroshchenko, T.; Radnik, J.; Schneider, M.; Rodemerck, U.; Linke, D.; Kondratenko, E.V. Bulk binary ZrO_2 -based oxides as highly active alternative-type catalysts for non-oxidative isobutane dehydrogenation. *Chem. Commun.* **2016**, *52*, 8164–8167. [[CrossRef](#)]
38. Han, S.; Zhao, Y.; Otroshchenko, T.; Zhang, Y.; Zhao, D.; Lund, H.; Vuong, T.H.; Rabéah, J.; Bentrup, U.; Kondratenko, V.A.; et al. Unraveling the Origins of the Synergy Effect between ZrO_2 and CrO_x in Supported CrZrO_x for Propene Formation in Nonoxidative Propane Dehydrogenation. *ACS Catal.* **2020**, *10*, 1575–1590. [[CrossRef](#)]
39. Kim, T.H.; Kang, K.H.; Baek, M.; Song, J.H.; Hong, U.G.; Park, D.S.; Choi, W.C.; Park, Y.-K.; Song, I.K. Dehydrogenation of propane to propylene with lattice oxygen over $\text{CrO}_y/\text{Al}_2\text{O}_3\text{-ZrO}_2$ catalysts. *Molec. Catal.* **2017**, *433*, 1–7. [[CrossRef](#)]
40. Kim, T.H.; Gim, M.Y.; Song, J.H.; Choi, W.C.; Park, Y.-K.; Hong, U.G.; Park, D.S.; Song, I.K. Deactivation behavior of $\text{CrO}_y/\text{Al}_2\text{O}_3\text{-ZrO}_2$ catalysts in the dehydrogenation of propane to propylene by lattice oxygen. *Catal. Commun.* **2017**, *97*, 37–41. [[CrossRef](#)]
41. Bugrova, T.A.; Mamontov, G.V. The Study of CrO_x -Containing Catalysts Supported on ZrO_2 , CeO_2 , and $\text{Ce}_x\text{Zr}_{(1-x)}\text{O}_2$ in Isobutane Dehydrogenation. *Kinet. Catal.* **2018**, *59*, 143–149. [[CrossRef](#)]
42. Otroshchenko, T.P.; Rodemerck, U.; Linke, D.; Kondratenko, E.V. Synergy effect between Zr and Cr active sites in binary CrZrO_x or supported $\text{CrO}_x/\text{LaZrO}_x$: Consequences for catalyst activity, selectivity and durability in non-oxidative propane dehydrogenation. *J. Catal.* **2017**, *356*, 197–205. [[CrossRef](#)]
43. Zhang, Y.; Zhao, Y.; Otroshchenko, T.; Han, S.; Lund, H.; Rodemerck, U.; Linke, D.; Jiao, H.; Jiang, G.; Kondratenko, E.V. The effect of phase composition and crystallite size on activity and selectivity of ZrO_2 in non-oxidative propane dehydrogenation. *J. Catal.* **2019**, *371*, 313–324. [[CrossRef](#)]
44. Otroshchenko, T.P.; Kondratenko, V.A.; Rodemerck, U.; Linke, D.; Kondratenko, E.V. Non-oxidative dehydrogenation of propane, n-butane, and isobutane over bulk ZrO_2 -based catalysts: Effect of dopant on the active site and pathways of product formation. *Catal. Sci. Technol.* **2017**, *7*, 4499–4510. [[CrossRef](#)]
45. Zhang, Y.; Zhao, Y.; Otroshchenko, T.; Lund, H.; Pohl, M.-M.; Rodemerck, U.; Linke, D.; Jiao, H.; Jiang, G.; Kondratenko, E.V. Control of coordinatively unsaturated Zr sites in ZrO_2 for efficient C–H bond activation. *Nat. Commun.* **2018**, *9*, 3794. [[CrossRef](#)]
46. Han, S.; Otroshchenko, T.; Zhao, D.; Lund, H.; Rockstroh, N.; Vuong, T.H.; Rabéah, J.; Rodemerck, U.; Linke, D.; Gao, M.; et al. The effect of ZrO_2 crystallinity in $\text{CrZrO}_x/\text{SiO}_2$ on non-oxidative propane dehydrogenation. *Appl. Catal. A Gen.* **2020**, *59025*, 117350. [[CrossRef](#)]
47. Cutrufello, M.G.; De Rossi, S.; Ferino, I.; Monaci, R.; Rombia, E.; Solinas, V. Preparation, characterisation and activity of chromia-zirconia catalysts for propane dehydrogenation. *Thermochim. Acta* **2005**, *434*, 62–68. [[CrossRef](#)]
48. Annuar, N.H.R.; Jalil, A.A.; Triwahyonoa, S.; Fatah, N.A.A.; The, L.P.; Mamat, C.R. Cumene cracking over chromium oxide zirconia: Effect of chromium(VI) oxide precursors. *Appl. Catal. A Gen.* **2014**, *475*, 487–496. [[CrossRef](#)]

49. Otroshchenko, T.; Sokolov, S.; Stoyanova, M.; Kondratenko, V.A.; Rodemerck, U.; Linke, D.; Kondratenko, E.V. ZrO₂-Based Alternatives to Conventional Propane Dehydrogenation Catalysts: Active Sites, Design, and Performance. *Angew. Chem. Int. Ed.* **2015**, *54*, 15880–15883. [[CrossRef](#)]
50. Mahmoud, H.R. Highly dispersed Cr₂O₃–ZrO₂ binary oxide nanomaterials as novel catalysts for ethanol conversion. *J. Mol. Catal. A Chem.* **2014**, *392*, 216–222. [[CrossRef](#)]
51. Baronskiy, M.G.; Kostyukov, A.I.; Larina, T.V.; Snytnikov, V.N.; Zaitseva, N.A.; Zhuzhgov, A.V. Photoluminescence of surface chromium centers in the Cr/Al₂O₃ system that is active in isobutane dehydrogenation. *Mater. Chem. Phys.* **2019**, *234*, 403–410. [[CrossRef](#)]
52. Cavani, F.; Koutyrev, M.; Trifiro, F.; Bartolini, A.; Ghisletti, D.; Iezzi, R.; Santucci, A.; Del Piero, G. Chemical and physical characterization of alumina-supported chromia-based catalysts and their activity in dehydrogenation of isobutane. *J. Catal.* **1996**, *158*, 236–250. [[CrossRef](#)]